



# Numerical Modeling of the Cavitation Flow in Throttle Geometry

M. Bambhania<sup>†</sup> and N. K. Patel

*Mechanical Engineering Department, Faculty of Technology & Engineering, The Maharaja Sayajirao University of Baroda, Vadodara, Gujarat, 390002, India*

<sup>†</sup>Corresponding Author Email: [mehul.bambhania-med@msubaroda.ac.in](mailto:mehul.bambhania-med@msubaroda.ac.in)

(Received June 14, 2022; accepted September 29, 2022)

## ABSTRACT

The modern fuel injectors work with ultra-high injection pressure with a micro-size nozzle, which inevitably triggers the cavitation flow inside the nozzle. The formation of vapor bubbles and their development inside the nozzle is difficult to characterize due to its highly fluctuating spatial and temporal parameters. The numerical models can predict the temporal behavior of cavitating flow with the real-size nozzle geometry, which is fairly expensive with the experiments. A systematic study has been carried out using throttle geometry to characterize the cavitation flow. The different turbulence, multiphase, and cavitation models are extensively evaluated and validated with experimental data. A combination of numerical models has been proposed to predict the cavitation flow more accurately with low computational time. The results obtained with the  $k-\omega$  SST (Shear Stress Transport) turbulence model and the ZGB (Zwart-Gerber-Belamri) cavitation model are more consistent with the experimental results. The overall structure of cavitation is well captured with both the VOF (Volume of Fluid) and the Mixture multiphase models. Although, the smaller structures like bubble formation and ligament breakup are only captured with the VOF (Volume of Fluid) tuned with the sharp interface method. The effect of pressure difference on the cavitation flow has been estimated with diesel and bio-diesel fuel. The effect of nozzle conicity on cavitation phenomena has also been reported.

**Keywords:** Cavitation; Fuel injection; Nozzle; Two-phase flow; CFD.

## NOMENCLATURE

### Symbols

$C_c$	contraction coefficient
$C_d$	discharge coefficient
$D$	throttle diameter
$K$	cavitation parameter
$\dot{m}$	mass flow rate
$n_0$	nuclei number density
$P$	pressure
$R$	bubble radius
$R_c$	rate of mass transfer for condensation
$R_e$	rate of mass transfer for evaporation
$U$	mixture velocity

### Greek letters

$\alpha$	volume fraction
$\sigma$	surface tension
$\rho$	density
$\mu$	dynamic viscosity

### Subscript

in	inlet
inj	injection
l	liquid
out	outlet
v	vapour

## 1. INTRODUCTION

The performance and emission characteristics of the diesel engine greatly depend upon the combustion process. The fuel atomization and spray characteristics are the governing parameters for efficient combustion. It is extensively acknowledged that the internal flow strongly

influence the spray formation and primary breakup. The primary breakup of liquid jets at the nozzle exit can be caused by a combination of three mechanisms (i) Aerodynamic forces acting on the liquid jet, (ii) Turbulence within the liquid phase (iii) Cavitation bubbles. During high-pressure injection, fuels flowing inside the fuel injector nozzle holes observed the cavitation

phenomenon. Therefore, it is required to understand cavitation phenomena and the parameter on which cavitation depends. There is significant progress in the clarification of the structure of cavitation flow inside the nozzle due to studies carried out by several researchers like Bergewerk (1959), Nurik (1976), Soteriou *et al.* (1995), Chaves *et al.* (1995), Schmidt *et al.* (1999), Arcoumanis *et al.* (2000), Winklhofer *et al.* (2001), Sou *et al.* (2008), Mauger *et al.* (2012), Payri *et al.* (2013). These studies throw light on the cavitation phenomena inside nozzles, in particular to the identification of a pattern of quasi-steady-state cavitation flow. There are different flow regimes observed during the cavitation flow. Initially, cavitation bubbles start to form at the nozzle entrance, known as cavitation inception. With injection pressure increased, the cavitation region develops and elongates to the outlet. This is referred to be super-cavitation. Further increase of injection pressure leads to entering the surrounding gas from the nozzle outlet and creates a thin layer of gas attached to the wall. This phenomenon is hydraulic flip. Experimental results have shown that the real flow does not always follow the classical scaling theory. The scale effect is caused by liquid quantity, bubble dynamics, geometrical differences due to wall roughness, specific flow regimes, cavitation nuclei, etc. However, the scale of the nozzle does not affect the discharge coefficient. Qualitative information in a real-size nozzle is essential to understand cavitation flow and its behavior fully. However, direct observation of cavitation flow in real conditions is difficult due to very small space and time parameters. To observe cavitation in a real-size nozzle, it must be transparent and capable of withstanding high injection pressure and choking condition. A good quality cavitation image will be convenient for the reader and model validation. Therefore several researchers have developed two-phase numerical models for cavitation flow. These models can predict the temporal behavior of cavitating flow with the real-size nozzle geometry, which is fairly expensive with the experiments. Nurik (1976) proposed a one-dimensional theoretical model to predict the discharge coefficient. The one-dimensional model is preferably good for predicting discharge co-efficient with a sharp inlet nozzle but does not give much detail about the internal flow behavior of the cavitation phenomena. An extensive multi-dimensional numerical model is required to gather information about flow parameters within the nozzle and at the outlet of the nozzle, which can later be used to model spray characteristics. Several researchers have developed two-phase numerical models for cavitation flow.

The classification of multi-dimensional cavitation modeling is not easy; broadly, it can be divided into two groups (i) Continuum or single-fluid models and (ii) Interface tracking or two-fluid models. Single fluid models require relatively less computation time and are a preferred approach for cavitation analysis. The mixture model and the Volume of Fluid (VOF) model are generally used to

simulate the multiphase flow. Both models consist of similar governing equations considering both phases simultaneously. The mixture model has one vapor fraction conservation equation which estimates the phase change process. The Volume of Fluid (VOF) model (proposed by Hirt and Nichols (1981)), apart from the Navier-Stokes equations and turbulence model equation, solved the equation of volume fraction. The summation of the two-phase volume fraction is equal to unity and thus satisfies the continuity equation. The mass transport model calculates the mass fraction of the gas. The mass transport model also referred to as the Baroclinic model, used the equation of state combined with a transport equation for liquid and gas volume fractions. A mass transport equation including a cavitation source term. This model is more precise and suitable for exploring the physical details of the cavitation phenomena and modeling the detachment of cavity bubbles. There is various mass transport model which has been proposed by researcher with different source term, i.e., Merkle *et al.* (1998), Kunz *et al.* (2000), Schnerr and Sauer (2001), Singhal *et al.* (2002), Zwart *et al.* (2004). In the two-fluid model, liquid and gas treat separately, and the governing equations are solved for both phases. This model can be divided into two approaches: i.e. the Eulerian-Eulerian approach and the Eulerian-Lagrangian approach. Yuan and Schnerr (2003), Alajbegovic *et al.* (2003), and Battistoni and Grimaldi (2010) used the Eulerian-Eulerian approach. Giannadakis *et al.* (2008) and Sou *et al.* (2014) used the Eulerian-Lagrangian approach. Due to significant improvements in computational processors, the use of commercial CFD tools has increased recently, which allows an understanding of the hydrodynamic behavior of the cavitation flow in detail. Experimental work published by Winklhofer *et al.* (2001) is mostly used for validation due to very comprehensive information in terms of quantitative as well as qualitative results. Mohan *et al.* (2014), Saha and Li (2016), Bambhania and Patel (2016), He *et al.* (2017), Sanmiguel Rojas *et al.* (2019) and Payri *et al.* (2021) validate their model or methods with Winklhofer's experimental data obtained for two-dimensional throttle geometry.

In the present study, the commercial CFD code ANSYS-Fluent is used to identify appropriate numerical models which can simulate the cavitation flow more accurately at a low computational cost. A systematic study has been carried out for cavitation flow. The nozzle geometry and boundary conditions are identical to Winklhofer *et al.* (2001) experimental work. The simulation has been carried out with k- $\epsilon$  RNG, k- $\epsilon$  REALIZABLE, and k- $\omega$  SST turbulent model. The SS and ZGB cavitation models are compared based on the vapor volume fraction. Finally, the mixture and the VOF multiphase model are used with dispersed and sharp interface capture options. The best-suited numerical model configuration has been suggested based on the above study. The second part includes the study of various parameters. The effect of pressure difference, nozzle k-factor, and fuel property on the cavitation flow has been discussed.

## 2. NUMERICAL MODELLING OF CAVITATION FLOW

### 2.1 One-dimensional Modelling of the Cavitation Flow

Nurik (1976) experimented with his transparent nozzle with varying upstream and downstream pressure and L/D ratios. Based on this work, he has proposed a one-dimensional theoretical model to predict discharge co-efficient given below:

$$C_d = C_c \sqrt{K} \quad (1)$$

$$K = \frac{P_{inj} - P_v}{P_{inj} - P_{back}} \quad (2)$$

Where  $K$  is the Cavitation parameter, and  $C_c$  is the contraction coefficient. The values of  $C_c$  depend on geometrical parameters; for the sharp edge nozzle, it is 0.61, and for the rounded corner, it is between 0.61 to 1. The value of  $C_c$  can be calculated with the help of the equation proposed by Weishbach (1882).

$$C_c = 0.63 + 0.37 \left( \frac{A_2}{A_1} \right)^3 \quad (3)$$

### 2.2 Multi-dimensional Modelling of the Cavitation Flow

In the single-fluid model, the two-phase flow is governed by a set of conservation equations of mass and momentum as given below:

$$\frac{\partial \rho}{\partial t} + \frac{\partial(\rho u_i)}{\partial x_i} = 0 \quad (4)$$

$$\frac{\partial(\rho u_i)}{\partial t} + \frac{\partial(\rho u_i u_j)}{\partial x_j} = -\frac{\partial p}{\partial x_i} + \frac{\partial}{\partial x_j} \left[ \mu_{eff} \left( \frac{\partial u_i}{\partial x_j} + \frac{\partial u_j}{\partial x_i} - \frac{2}{3} \frac{\partial u_i}{\partial x_i} \right) \right] \quad (5)$$

The volume fraction of the liquid phase is used to calculate the mixture density and mixture viscosity.

$$\rho = (1 - \alpha_l) \rho_v + \alpha_l \rho_l \quad (6)$$

$$\mu = (1 - \alpha_l) \mu_v + \alpha_l \mu_l \quad (7)$$

Where  $\rho_v$  and  $\rho_l$  are the vapor phase and liquid phase density, and  $\mu_v$  and  $\mu_l$  are the vapor phase and liquid phase viscosity, respectively. The effective viscosity ( $\mu_{eff}$ ) in equation (5) is the summation of the molecular viscosity ( $\mu_m$ ) and turbulent viscosity ( $\mu_t$ ). The turbulent viscosity can be calculated by:

$$\text{k-}\epsilon \text{ models} \quad \mu_t = C_\mu \rho \frac{k^2}{\epsilon} \quad (8)$$

$$\text{k-}\omega \text{ models} \quad \mu_t = \alpha \rho \frac{k}{\omega} \quad (9)$$

A source term is required in the mass transport equation to evaluate the phase change between liquid and vapor with this model.

$$\frac{\partial(\alpha_l \rho_l)}{\partial t} + \nabla \cdot (\alpha_l \rho_l U) = R_c + R_e \quad (10)$$

where  $R_c$  and  $R_e$  are the source term to calculate the rate of mass transfer for condensation and

evaporation, respectively.  $U$ ,  $\alpha_l$ , and  $\rho_l$  are mixture velocity, the volume fraction of liquid and density of liquid respectively. If there is no mass transfer between phases, RHS is zero, the transport equation for the Volume of Fluid (VOF) model. The volume fraction of the vapor phase ( $\alpha_v$ ) is calculated by:

$$\alpha_v = 1 - \alpha_l = \frac{\frac{4}{3} \pi R_b^3 n_0}{1 + \frac{4}{3} \pi R_b^3 n_0} \quad (11)$$

Where  $R_b$  and  $n_0$  denote the bubble radius and bubble nuclei number density (bubble concentration per unit volume). The growth and collapse of the bubbles can be calculated by using the Rayleigh-Plesset (RP) bubble dynamic equation.

$$R \frac{d^2 R}{dt^2} + \frac{3}{2} \left( \frac{dR}{dt} \right)^2 + \frac{4\mu}{R} \frac{dR}{dt} + \frac{2\sigma}{\rho R} = \frac{P_v - P_\infty}{\rho} \quad (12)$$

Where  $R$  is the bubble radius,  $\frac{dR}{dt}$  is the bubble wall velocity,  $\sigma$  is the surface tension, and  $P_v$  is the vapor pressure. The RP equation considers vapor pressure ( $P_v$ ) as a threshold for evaporation and condensation. The mass transfer rate is given in the table below using the RP equation.

**Table-1 Different mass transfer source terms for condensation and evaporation**

Evaporation ( $P_L < P_V$ )		
Schnerr and Sauer (2001)	$R_e = -C_v \frac{3\rho_l \rho_v \alpha_l (1-\alpha_l)}{\rho_m R_b} \text{sgn}(P_l - P_v) \sqrt{\frac{2 P_l - P_v }{3\rho_l}}$	(13)
Zwart et al.(2004)	$R_e = F_{vap} \frac{3\alpha_{nuc} \rho_v (1-\alpha_v)}{R_b} \sqrt{\frac{2 P_l - P_v }{3\rho_l}}$ ( $F_{vap}=50$ )	(14)
Condensation ( $P_V < P_L$ )		
Schnerr and Sauer (2001)	$R_c = C_c \frac{3\rho_l \rho_v \alpha_l (1-\alpha_l)}{\rho_m R_b} \text{sgn}(P_v - P_l) \sqrt{\frac{2 P_l - P_v }{3\rho_l}}$	(15)
Zwart et al.(2004)	$R_c = F_{con} \frac{3n_0 \rho_v}{R_b} \sqrt{\frac{2 P_l - P_v }{3\rho_l}}$ , ( $F_{con}=0.01$ )	(16)

## 3. MODEL VALIDATION

### 3.1 Winklhofer Throttle Geometry

Qualitative information in a real-size nozzle is essential to understanding cavitation flow and its complete behavior. However, direct observation of cavitation flow in the real condition is difficult due to very small space and time parameters. To observe cavitation in a real-size nozzle, it must be transparent and capable of withstanding high injection pressure and choking condition. A good quality cavitation image will be convenient for the

reader and model validation. Winklhofer *et al.* (2001) experimented with a real-sized two-dimensional throttle (transparent rectangular cross-section) working with European diesel fuel, as shown in Fig.1.



**Fig. 1. Two-dimensional throttle (transparent rectangular cross-section) geometry.**

Optical methods were developed and applied to diagnose high-pressure diesel flow at transient conditions using interferometry imaging shown in Fig. 2. They use three different nozzles named J, U, and W throttle with different outlet contractions, i.e., 0 %, 5 % and 10 %, respectively. They measured values of the mass flow rate of diesel at different pressure drops and predicted cavitation inception and choking conditions. In the present study, identical geometry and boundary condition has been used to analyze the cavitation flow inside the nozzle as shown in Fig. 3. The density of diesel's liquid and vapor phases are considered  $830 \text{ kg/m}^3$  and  $9.4 \text{ kg/m}^3$ , respectively. The viscosity of liquid and vapor phases are considered as  $0.00336 \text{ kg/ms}$  and  $7.006 \times 10^{-6} \text{ kg/ms}$ , respectively.

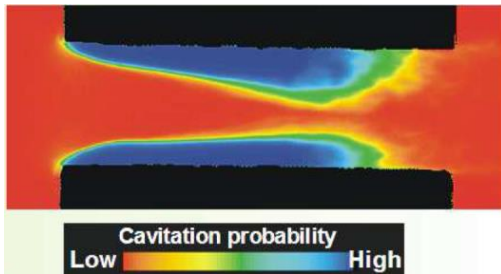


**Fig. 2. Cavitation field using Interferometry imaging.**

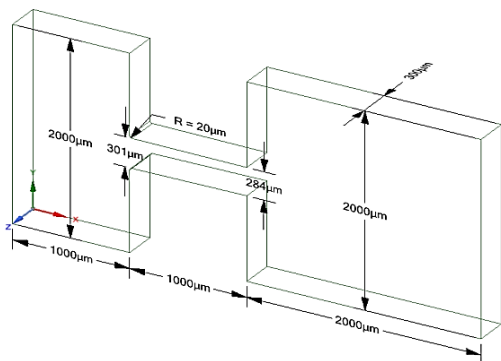


**Fig. 3. Computational domain with its dimension.**

### 3.2 Grid Generation

The computational domain was discretized using a cut-cell method with structural Hexa-hedral mesh elements. The specific mesh refinement treatment has been performed near the nozzle inlet corner, as shown in Fig. 4. The results of the CFD simulation depend on the computational grid quality and size. Therefore it is important to resolve the grid to the extent that the solution becomes independent of the grid size. However, there is a balance required between grid refinement and computational cost. The grid independence test has been performed and the results of the mass flow rate of fuel are shown in Fig. 5. It is observed that the variation in the calculated mass flow rate is least with 299324 elements. Further refinement in the mesh would not affect the orthogonal quality and aspect ratio of the grid. Hence considering the best compromise between the consistency of results and computational cost, 299324 mesh elements have been chosen for the further simulation study.

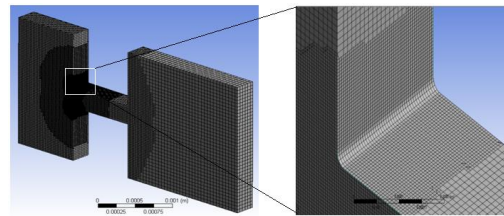


**Fig. 4. Grid generation with refinement at throttle inlet.**

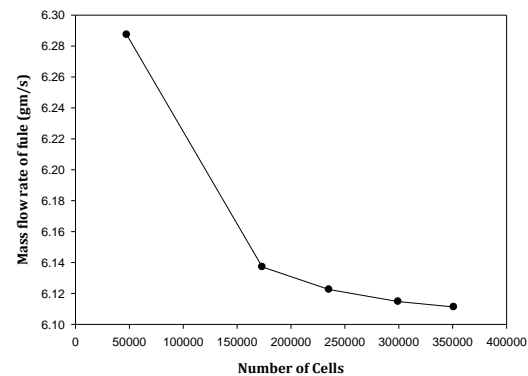


**Fig. 5. Effect of Grid on the mass flow rate of fuel.**

### 3.3 Numerical Set-up

The fuel is injected at a constant pressure of 100 bar and varied the outlet pressure from 15 bar to 80 bar. No-slip boundary condition has been employed to the wall. The turbulence intensity and hydraulic diameter are defined at the inlet and outlet of the nozzle. The finite volume approach has been used with commercial CFD software ANSYS-Fluent. The pressure-based segregated algorithm has been used to solve the governing equation. The pressure-velocity coupling has been solved by the Coupled algorithm. The special discretization of the pressure is done by using PRESTO! Method. The second-order upwind scheme is used for the momentum

equation. The volume fraction and turbulent kinetic energy are discretised by the first-order upwind scheme. During the transient simulation, the Corant number is set as 0.25 with minimum and maximum time step sizes of  $10^{-8}$  sec to  $10^{-6}$  sec respectively. The convergence criteria for the governing equation are set to  $10^{-6}$ . The under-relaxation factor has been adjusted (between 0 and 1) to ensure the solution's stability.

### 3.4 Model Validation

To validate this numerical setup, comparisons were made between the results of simulations and that of an actual experiment by *Winkhofer et al. (2001)*. Quantitative and Qualitative validation have been shown in Fig. 6, 7 and 8. A range of pressure differences has been used to calculate the mass flow rate of fuel. Present results show good agreement with the experimental data of *Whinklhofer et al. (2001)*. with a maximum error of 7%. It can be attributed to the assumptions taken in simulations and material properties variations. But simulation results hold a good trend following experimental results. Fig. 7 shows the velocity profile at a  $53 \mu\text{m}$  distance from the inlet of the nozzle for the pressure difference of 67 bar and 85 bar, which are compared with experimental data. This study observes mass flow rate calculated is higher than the experimental claim, which results in the velocity profile being over-predict for both cases. In the experimental images, the red color indicates the liquid fraction and blue color used for the vapor; a similar color map is used for validation purposes, as shown in Fig. 8. It is observed that the numerical model accurately predicts the inception of cavitation, although, with a large pressure difference, it under predicts the extent of the cavitation zone. The results obtained in the experimental work are the integrated effect of the light transmitted through the two-phase flow. However, the current results belong to a single plane in the fluid domain.

## 4. RESULTS AND DISCUSSION

### 4.1 Assessment of Turbulence Model

There are three turbulence models, i.e., (1)  $k-\epsilon$  RNG (Renormalization Group), (2)  $k-\epsilon$  REALIZABLE (3)  $k-\omega$  SST (Shear Stress Transport), which have been tested to capture cavitation and compared with available experimental results. The  $k-\epsilon$  model is more suitable for the shear-free region, however,  $k-\omega$  provides a more accurate solution near the wall region. In the  $k-\omega$  SST model, the features of both  $k-\epsilon$  and  $k-\omega$  are integrated, which automatically activates  $k-\epsilon$  and  $k-\omega$  over the domain. Therefore, the  $k-\omega$  SST model is likely to perform well in the near-wall zone. The recirculation and shear zone will increase with a pressure drop at the nozzle entry. The  $k-\epsilon$  RNG,  $k-\epsilon$  realizable turbulence model perform weak in the shear zone and underpredicts the cavitation intensity shown in Fig. 9. It is observed that results with the  $k-\omega$  SST turbulent model show consistency with experimental results. It is also

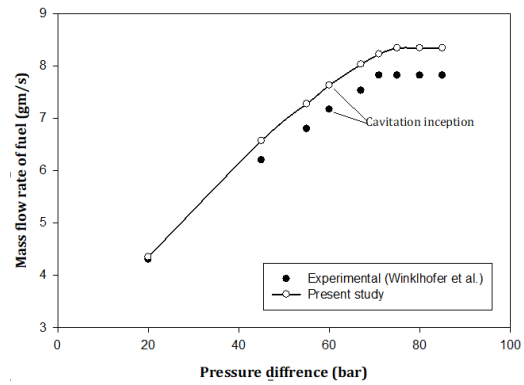


Fig. 6. Quantitative comparison of fuel mass flow rate with experimental results.

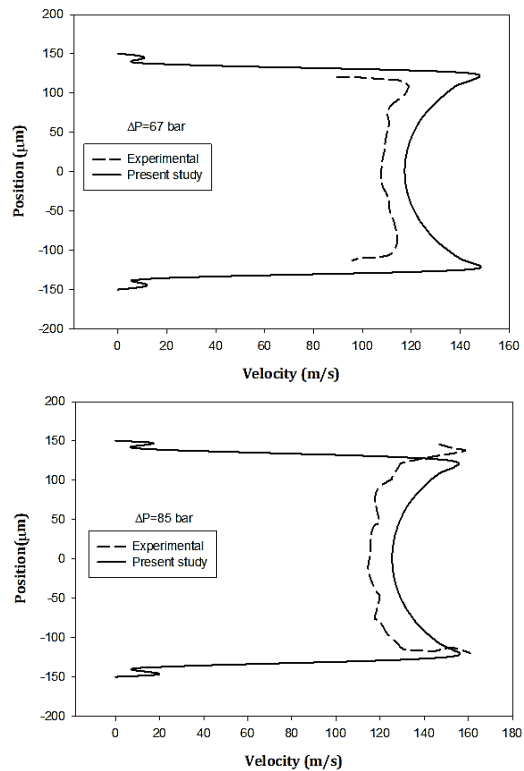


Fig. 7. Comparison of the velocity profiles at  $53 \mu\text{m}$  from the nozzle inlet.

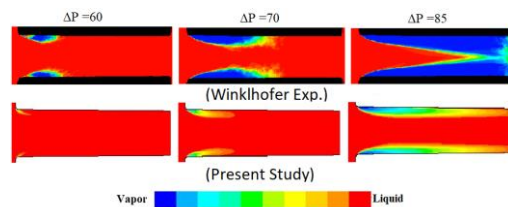


Fig. 8. Qualitative comparison of Liquid volume fraction with Winkhofer's experimental results.

reasonably good with a wide range of flows. The mass flow rate of fuel has been calculated at variable pressure conditions and compared with experimental data as shown in Fig. 10. The nozzle's choking indicates only with the  $k-\omega$  SST model;

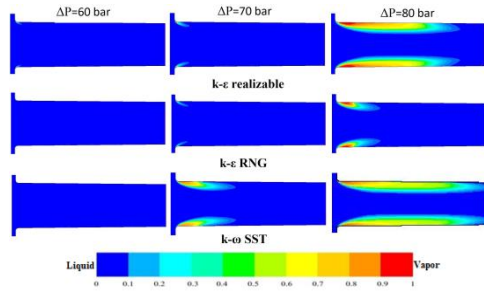


Fig. 9. Volume fraction of Vapour at with different of Turbulence model.

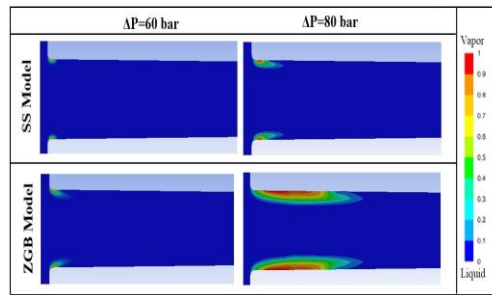


Fig. 11. Comparison of the SS and the ZGB cavitation model based on the volume fraction of vapor.

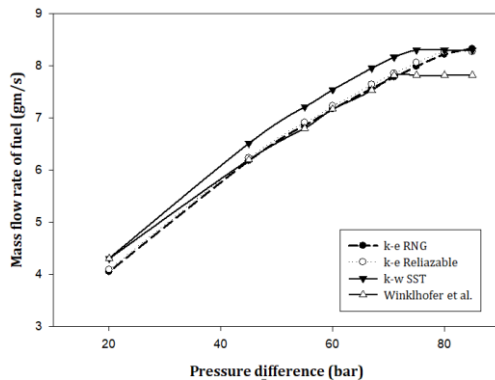


Fig. 10. Comparison of turbulence model based on the mass flow rate of fuel.

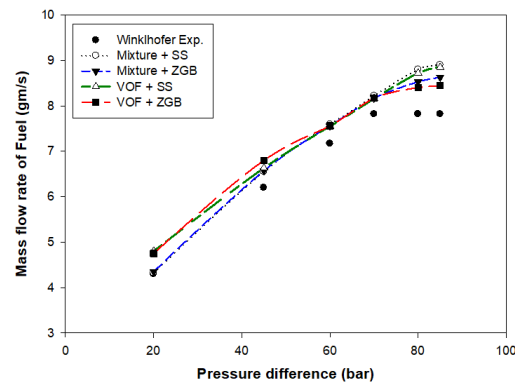


Fig. 12. Comparison of the predicted mass flow rate with the Mixture and VOF multiphase model in the SS and ZGB cavitation model combination at different pressure differentials.

other turbulence models fail to determine choking. It is concluded that the  $k-\omega$  SST model is preferred to simulate cavitation flow and is used in further simulation work.

#### 4.2 Assessment of Cavitation Model

The two cavitation models, i.e. (1) SS (Schnerr and Sauer) model and (2) ZGB (Zwart-Gerber-Belamri) model, is compared. It has been seen through the results that the SS cavitation model is inaccurate as it fails to capture cavitation inception at a pressure difference of 60 bar. The methodology adopted for the source term formulation leads to the poor performance of the SS model. In the SS model  $n_B$ , the bubble density per unit volume of liquid is to be considered as  $10^{-13}$  for the best result. The ZGB contain many tuning parameters that provide better results. The higher initial vaporization constant in the ZGB model gives a more vapor fraction as compared to the SS model. The evaporation and condensation rate in the ZGB model is linear, however, in the SS model, it is non-linear. With the ZGB model, cavitation inception appears at a pressure difference of 60 bar, which supports the experimental data shown in Fig. 11.

The SS cavitation model over-predicts the mass flow rate of fuel over the range of pressure difference, as shown in Fig. 12. This is expected since the SS model underpredicts the cavitation region at a higher pressure difference. However, the ZGB model exhibits good qualitative and quantitative results with experimental data. Based on this study, it is concluded that the ZGB is a preferred cavitation model.

#### 4.3 Assessment of Multi-phase model and Interface modeling

The volume of fluid (VOF) is a surface tracking model designed for two immiscible fluids where the interface is required to capture. The mixture model differs from the VOF model in two aspects (i) the mixture model allows for movement of the phases with different velocities by considering the concept of slip velocity. (ii) the mixture model also allows the interpenetrating of mass, momentum, and energy between the phases. The mixture and VOF multiphase model have been used in conjunction with the SS and ZGB cavitation model. The simulation has been carried out to calculate the fuel mass flow rate at variable pressure differences and compared with Winklhofer *et al.* (2001) experimental results. Typically all combinations overpredict the mass flow rate compared to experimental results, as shown in Fig. 13. The mass flow rate prediction by the ZGB cavitation model with both the mixture and VOF is better than those with the SS

cavitation model. Particularly, at the higher pressure difference, the VOF with the ZGB precisely predicts the trend of choked flow. Although the SS cavitation model fails to predict chocking, mass flow rate increases continuously with pressure for both mixture and VOF model. No significant difference was observed in the qualitative comparison of cavitation flow with the mixture and

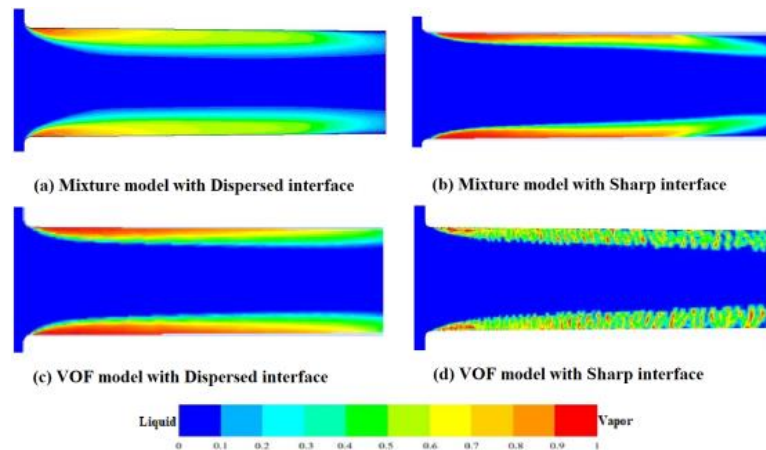


**Fig. 13.** Comparison of vapor fraction contour between the mixture and VOF model in conjunction with dispersed and sharp interface option at  $\Delta P=85$  bar.

VOF model. In extension, the dispersed and sharp interface approach with the mixture and VOF model is implemented in ANSYS-FLUENT. A comparison between the prediction from the two model mixture and VOF (with different interphase approach) are shown in Fig.13. The mixture model works better with the dispersed option and does not show a major difference with the sharp interface option. The VOF model will better capture the interface for a given mesh resolution shown in Fig 13 (d). It is observed that the overall structure of cavitation is well captured with both models. Although, the smaller structures like bubble formation and ligament breakup are only captured with the VOF sharp interface option. This is due to consideration of the effect of surface tension in the VOF model.

#### 4.4 Transient Simulation

The cavitation flows involved continuous bubble growth and collapse; they also travelled toward the outlet of the nozzle. Such phenomena must be solved using a time-dependent formulation. The transient simulation has been carried out with a pressure difference of 85 bar. The time step during the simulation is kept at  $10^{-7}$  s with the VOF+ZGB model with a sharp interface option. The mechanism of bubble formation and its movement inside the nozzle is shown in Fig. 14. The inception of cavitation begins after  $10\mu s$  at the round corner of the throttle inlet. As time proceeds, the cavitation region moves downstream and fully develops up to  $100\mu s$ . The bubble breakup and ligament formation are visible in the vapor fraction contour. The results obtained at the throttle outlet predict the fuel's primary breakup. This is very useful information for coupling inner throttle flow and spray formation.

#### 4.5 Summary of Numerical Modelling of Cavitation Flow

The accuracy of the numerical solution depends on the appropriate section model and sub-model. The main idea behind this work is to identify the best-suited numerical model for the cavitation flow. The proposed model must be accurate and

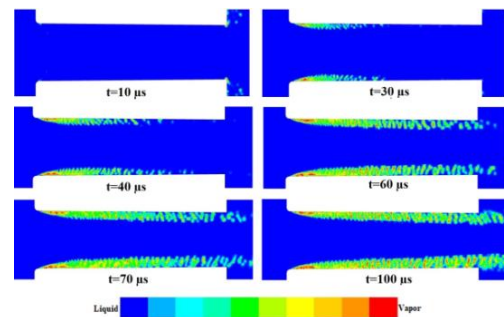


**Fig. 14.** Vapour bubble formation and its development inside the throttle at  $\Delta P=85$  bar.

computationally less costly. The cavitation phenomenon involved gas-liquid flow which is turbulent. A systematic study has been carried out with three different turbulence models, two cavitation models and two multiphase models. The results of the mass flow rate of fuel have been compared with experimental data. The maximum error with different combinations of the model has been calculated and reported in Fig. 15. The combination of the VOF+ZGB+  $k-\omega$  SST exhibits the least error among all cases. Moreover, LES based turbulence model is widely adopted to capture the detail of bubble and ligament formation. In the present work, the VOF is tuned with a sharp interface capturing method using the  $k-\omega$  SST turbulence model. The present method required substantially low computational time as compared to the similar work reported by [Sanmiguel Rojas et al. \(2019\)](#) using LES.

## 5. PARAMETRIC STUDY

### 5.1 Effect of Pressure Difference

In the present study followed by [Winklhofer et al. \(2001\)](#) experiment, pressure difference has been set similarly. Injection pressure is kept constant at 100 bar for all cases, and backpressure varies from 15 bar to 80 bar, which provides a pressure difference range from 20 bar to 85 bar. The

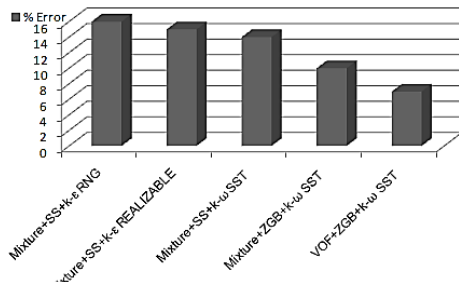


**Fig. 15. % Error mass flow rate of the fuel with different combinations of numerical models.**

efficiency of the throttle can be decided based on the discharge coefficient, which is calculated by:

$$C_d = \frac{\dot{m}_{actual}}{A\sqrt{2\rho(\Delta P)}} \quad (17)$$

The fuel mass flow rate and the discharge coefficient have been calculated from simulation results at variable pressure differences. Discharge coefficient vs. Cavitation parameter has been obtained to compare present results with Nurik's one-dimensional theoretical model (Referred equation 1), as shown in Fig. 16. It is observed that the discharge coefficient decreases after cavitation inception and reaches its minimum value at supercavitation. Since the throttle has been choked after supercavitation, no further mass flow rate increases with pressure differences. It is interesting to note that the present data falls above the theoretical curves. This suggests the effect of rounding at the inlet increases the discharge coefficient. Nurik's theoretical model is based on the experimental work carried out with a sharp edge nozzle, which exhibits early cavitation inception ( $K=2$ ). In Nurik's experiment, he observed hydraulic flip instead of supercavitation, which was the reason for the lower values of discharge coefficient. A higher value of the cavitation parameter indicates the smaller differences between the injection pressure and backpressure, which is non-cavitation flow. During non-cavitating flow, the discharge coefficient is no longer a function of the cavitation parameter but depends on the Reynolds number. At a higher cavitation parameter value, the discharge coefficient stays fairly constant.

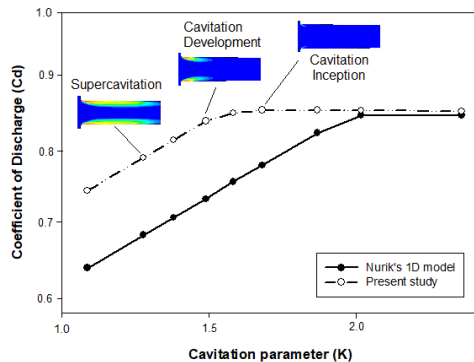


**Fig. 16. Comparison of Discharge coefficient vs. Cavitation parameter with Nurik's theoretical model.**

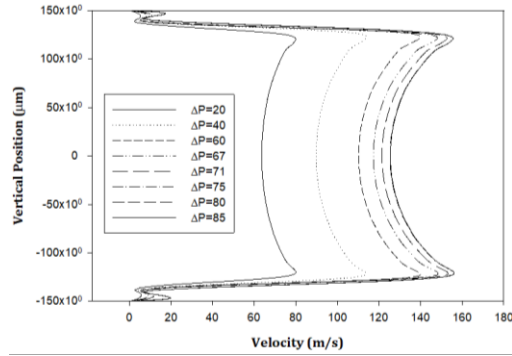


**Fig. 17. Velocity profile at a location  $x=0.053\text{mm}$  from the nozzle inlet.**

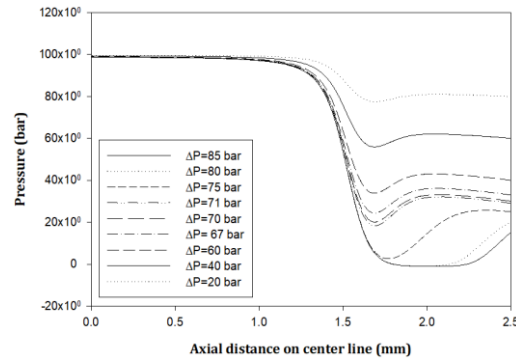


**Fig. 18. Pressure distribution along with the axial distance.**

Large recirculation is forming near the entrance due to sudden contraction in the area. This recirculation zone creates a shear layer and low-pressure region, which ultimately initiate the vapor bubble formation at the throttle entrance. The velocity profile in the transverse direction at a location of 0.053 mm from the throttle entrance is shown in Fig. 17. The peak velocity occurs in the shear layer, approximately 0.045mm far from the top and bottom wall; again, it decreases to a minimum value at the center. The size of the shear layer extended with the increase in the pressure differences. The pressure distribution along the center line is shown in Fig. 18. As the pressure difference increases, the low-pressure recirculation zone extends toward the throttle outlet.

### 5.2 Effect of Nozzle Geometry

The conicity factor or  $k$ -factor has been used to evaluate the effects of nozzle geometry. Here  $k$ -factor measures the amount of taper and is defined as:

$$k - factor = \frac{D_{in} - D_{out}}{D_{in}} \times 100 \quad (18)$$

Where  $D_{in}$  and  $D_{out}$  are inlets and exit diameters of a nozzle in a micrometre, respectively, the positive  $k$ -factor represents the convergent nozzle, and the negative  $k$ -factor represents the divergent nozzle. The dimensions chosen are one of the experimental studies of *Winklhofer et al. (2001)*, all geometries were kept with a constant inlet diameter of 301  $\mu\text{m}$ . The nozzle with zero  $k$ -factor has the same inlet and exit diameters. In positive  $k$ -factor, exit diameter is 284  $\mu\text{m}$  making  $k$ -factor = +5.65. Similarly, the

negative  $k$ -factor exit diameter was kept at 318  $\mu\text{m}$  with  $k$ -factor = -5.65. Generally, nozzles of positive and zero  $k$ -factor are used in the fuel injector. Since the negative  $k$ -factor nozzle is divergent and tends to reduce exit velocity, which may lead to poor atomization.

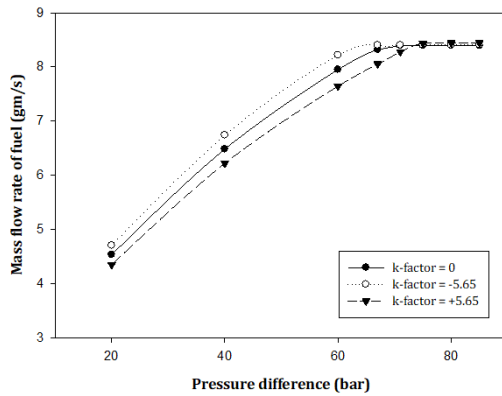


**Fig. 19. Effect of  $k$ -factor on the mass flow rate of fuel at a variable pressure difference.**

The effects of nozzle convergence on the mass flow rate are shown in Fig. 19. It is observed that the mass flow rate of the divergent nozzle is more than the convergent nozzle before cavitation inception. But this condition reverses after getting choked flow. As soon as the choking condition approaches, the area available to liquid is less in the divergent nozzle due to the thick cavitation layer, as shown in Fig. 20. But this is not the case in the convergent-shaped nozzle. The inertia of liquid wipes out the developed cavitation layer and maintains a thin layer. Hence, the available area in the case of the convergent nozzle at the choking condition is more than the divergent nozzle.

### 5.3 Effect of Fuel Properties

The scarcity of petroleum and continuously increasing emissions encourage the use of bioproducts. Biofuels are renewable, and that is the major advantage of it. Bio-diesel is a greener

alternative to diesel. Due to its properties, its usage is limited. Here a study shows the effects of bio-diesel over cavitation phenomena. It is observed that the inception of cavitation in the case of diesel appears at a lower pressure difference ( $\Delta P=60$  bar) compared to bio-diesel (at  $\Delta P=67$  bar) shown in Fig 21. Due to higher liquid viscosity and lower saturation pressure, bio-diesel lags in cavitation inception. Due to the higher density of bio-diesel, its overall mass flow rate and discharge coefficient are more than diesel for the same pressure difference shown in Fig. 21.

## 6. CONCLUSIONS

In this work, a systematic study has been carried out to investigate cavitation flow in the throttle type geometry. The diesel fuel has been injected at 100 bar pressure through the tapered throttle with inlet and outlet diameters of 0.301mm and 0.284mm, respectively. The accurate sets of the numerical models have been identified in ANSYS-Fluent for simulating the cavitation flow. The different turbulence, multiphase, and cavitation model has been used, tested, and compared with the experimental data of Winklhofer *et al.* (2001). Based on this following conclusions and recommendations are derived:

- Cavitation inception has been noticed at 60 bar of pressure difference; the numerical model accurately predicts this event. Although a large pressure difference, it underpredicts the extent of the cavitation zone.
- Choking off the throttle has been observed after the 70 bar pressure difference. The mass flow rate of the fuel is calculated and compared with experimental data, which shows a maximum of 7% error. The trend followed by the  $k$ - $\omega$  SST model is closely matched with experimental results. The nozzle's choking indicates only with the  $k$ - $\omega$  SST model; other turbulence models fail to determine choking.

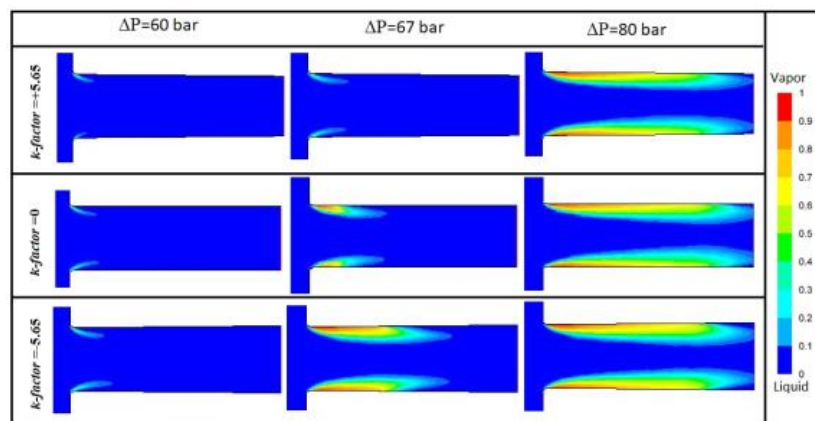


**Fig. 20. Comparison of the vapor fraction contour at different  $k$ -factor values.**

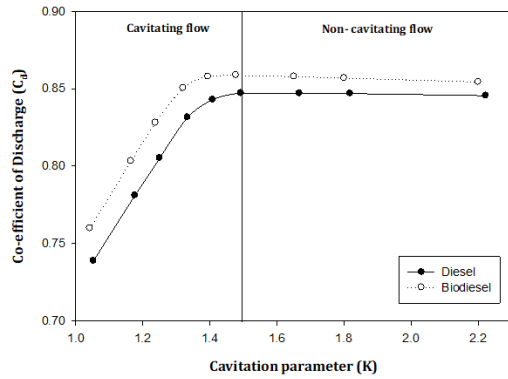


**Fig. 21. Effect of cavitation number on discharge coefficient for diesel and bio-diesel.**

- The SS cavitation model over-predicts the mass flow rate of fuel over the range of pressure difference. The ZGB model exhibits good qualitative and quantitative results with experimental data.
- It is observed that the overall structure of cavitation is well captured with both VOF and the mixture models. Although, the smaller structures like bubble formation and ligament breakup are only captured with the VOF sharp interface option. This is due to consideration of the effect of surface tension in the VOF model.
- The inception of cavitation begins after  $10\mu\text{s}$  at the round corner of the throttle inlet. As time proceeds, the cavitation region moves downstream and is fully developed up to  $100\mu\text{s}$ .
- It is observed that the discharge coefficient decreases after cavitation inception and reaches its minimum value ( $C_d=0.85$ ) at super cavitation, which consistence with Nurik's theoretical model.
- The velocity profile in the transverse direction at  $0.053\text{ mm}$  from the throttle entrance shows peak velocity ( $155\text{ m/s}$ ) in the shear layer approximately at  $0.045\text{ mm}$  far from the top and bottom wall.
- The mass flow rate of the divergent nozzle is more than the convergent d nozzle before cavitation inception. But this condition reverses after getting choked flow. As soon as the choking condition approaches, the area available to liquid is less in the divergent nozzle due to the thick cavitation layer.
- It is observed that the inception of cavitation in the case of diesel appears at a lower pressure difference ( $\Delta P=60\text{ bar}$ ) compared to bio-diesel (at  $\Delta P=67\text{ bar}$ ). With higher liquid viscosity and lower saturation pressure, bio-diesel lags in cavitation inception.

## REFERENCE

- Arcoumanis, C., H. Flora, M. Gavaises and M. Badami (2000). Cavitation in real-size multi-hole diesel injector nozzles. *SAE Transactions* 1, 1485-500.
- Alajbegovic, A., D. Greif, B. Basara and U. Iben (2003, Sept). Cavitation calculation with the two-fluid model. *3rd European-Japanese Two-Phase Flow Group Meeting*, Certosa di Pontignano.
- Bambhania, M. and N. Patel (2016, June) Numerical simulation to predict cavitation inside diesel engine fuel injector nozzle. *International conference on Multidisciplinary Research Approach for the accomplishment of academic excellence in Higher technical education through industrial practices*, Bangkok.
- Battistoni, M. and C. N. Grimaldi (2010, Jan). Analysis of transient cavitating flows in diesel injectors using diesel and biodiesel fuels. *SAE International Journal of Fuels and Lubricants* 1, 3(2), 879-900.
- Bergwerk, W. (1959). Flow pattern in diesel nozzle spray holes. *Proceedings of the Institution of Mechanical Engineers* 173(1), 655-60.
- Chaves, H., M. Knapp, A. Kubitzek, F. Obermeier and T. Schneider (1995, Jan). Experimental study of cavitation in the nozzle hole of diesel injectors using transparent nozzles. *SAE Transactions* 1, 645-57.
- Giannadakis, E., M. Gavaises and C. Arcoumanis (2008) Modelling of cavitation in diesel injector nozzles. *Journal of Fluid Mechanics* 616, 153-93.
- He, Z., L. Zhang, K. Saha, S. Som, L. Duan and Q. Wang (2017). Investigations of effect of phase change mass transfer rate on cavitation process with homogeneous relaxation model. *International Communications in Heat and Mass Transfer* 1(89) 98-107.
- Hirt, C. W. and B. D. Nichols (1981). Volume of Fluid (VOF) method for the dynamics of free boundaries. *Journal of Computational Physics* 39(1), 201-25.
- Kunz, R. F., D. A. Boger, D. R. Stinebring, T. S. Chyczewski, J. W. Lindau, H. J. Gibeling, S. Venkateswaran and T. R. Govindan (2000). A preconditioned Navier–Stokes method for two-phase flows with application to cavitation prediction. *Computers and Fluids* 29(8):849-75.
- Mauger, C., L. Mees, M. Michard, A. Azouzi and S. Valette (2012). Shadowgraph, Schlieren and interferometry in a 2D cavitating channel flow. *Experiments in Fluids* 53(6), 1895-913.
- Merkle, C. L., J. Feng and P. E. Buelow (1998). Computational modelling of the dynamics of sheet cavitation. *Proceeding of the 3rd*

- International Symposium on Cavitation*, Grenoble, France.
- Mohan, B., W. Yang and S. Chou (2014). Cavitation in injector nozzle holes—a parametric study. *Engineering Applications of Computational Fluid Mechanics* 8(1), 70-81.
- Nurik, W. H. (1976). Orifice cavitation and its effect on spray mixing. *ASME Journal of Fluids Engineering* 98(4), 681–687.
- Payri, R., J. Gimeno, P. Marti-Aldaraví and M. Martinez (2021) Validation of a three-phase Eulerian CFD model to account for cavitation and spray atomization phenomena. *Journal of the Brazilian Society of Mechanical Sciences and Engineering* 43(4), 1-5.
- Payri, R., F. J. Salvador, J. Gimeno and O. Venegas (2013) Study of cavitation phenomenon using different fuels in a transparent nozzle by hydraulic characterization and visualization. *Experimental Thermal and Fluid Science* 1(44), 235-44.
- Saha, K. and X. Li (2016) Assessment of cavitation models for flows in diesel injectors with single-and two-fluid approaches. *Journal of Engineering for Gas Turbines and Power* 1, 138(1).
- Sanmiguel Rojas, E., P. Gutierrez-Castillo, C. del Pino and J. A. Auñón-Hidalgo (2019) Cavitation in transient flows through a micro-nozzle. *Journal of Fluids Engineering* 1, 141(9).
- Schmidt, D. P., C. J. Rutland, M. L. Corradini P. Roosen and O. Genge (1999). Cavitation in asymmetric two-dimensional nozzles. *Journal of Engines*. 108(3):613-29.
- Schnerr, G. H. and J. Sauer (2001, May) Physical and numerical modeling of unsteady cavitation dynamics. *Fourth international Conference on Multiphase Flow*, Vol. 1, ICMF, New Orleans.
- Singhal, A. K., M. M. Athavale, H. Li and Y. Jiang (2002). Mathematical basis and validation of the full cavitation model. *Journal of Fluids Engineering* 124(3), 617-24.
- Soteriou, C., R. Andrews and M. Smith (1995). Direct injection diesel sprays and the effect of cavitation and hydraulic flip on atomization. *SAE Transactions* 1, 128-53.
- Sou, A., B. Bicer and A. Tomiyama (2014) Numerical simulation of incipient cavitation flow in a nozzle of a fuel injector. *Computers and Fluids*. 103, 42-8.
- Sou, A., M. I. Maulana, S. Hosokawa and A. Tomiyama (2008). Ligament formation induced by cavitation in a cylindrical nozzle. *Journal of Fluid Science and Technology* 3(5), 633-44.
- Weishbach, J. (1882). *Mechanics of engineering: Theoretical mechanics, with an introduction to the calculus*. D. Van Nostrand.
- Winklhofer, E., E. Kull, E. Kelz and A. Morozov (2001, Sep.) Comprehensive hydraulic and flow field documentation in model throttle experiments under cavitation conditions. *Proceedings of the ILASS-Europe Conference*, Zurich, 574-579.
- Yuan, W. and G. N. Schnerr (2003, Nov.) Numerical simulation of two-phase flow in injection nozzles: Interaction of cavitation and external jet formation. *Journal of Fluids Engineering* 125(6), 963-9.
- Zwart, P. J., A. G. Gerber and T. Belamri (2004, May) A two-phase flow model for predicting cavitation dynamics. *In Fifth International Conference on Multiphase Flow*, Yokohama, Japan Vol. 152.